**Impact of Tropical SST Anomalies on West African Rainfall.**

T. Losada (1), B. Rodriguez-Fonseca (1,2), E. Mohino (1), J. Bader (3,4), S. Janicot (5), and C. R. Mechoso (6)

(1) Departamento de Física de la Tierra, Astronomía y Astrofísica I, Geofísica y Meteorología. UCM, Av. Complutense s/n, 28040 Madrid (Spain).

(2) Instituto de Geociencias (CSIC-UCM), Facultad de CC. Físicas, Plaza de Ciencias 1, 28040 Madrid (Spain)

(3) Max-Planck-Institut fuer Meteorologie, Hamburg (Germany).

(4) Bjerknes Centre for Climate Research, Allegaten 70, 5007 Bergen (Norway).

(5) LOCEAN/IPSL, IRD, Université Pierre et Marie Curie, Paris (France).

(6) Department of Atmospheric Sciences, University of California, Los Angeles, CA 90095 (USA).

E-mail: tldoval@fis.ucm.es

**Abstract**

Previous works have addressed the impact on Sahelian rainfall of sea surface temperature (SST) anomalies in the tropical Pacific, Indian and Atlantic Oceans. Some of them have found these impacts to be non-stationary with important differences before and after the 1970's.

This paper re-examines the problem and its non-stationarity. In the period 1970-present a mode of covariability develops between rainfall in West Africa and SSTs over the entire tropics. Accordingly, an increase of summer rainfall in that region corresponds to an oceanic pattern that resembles a Pacific Niña - Atlantic Niño – western Indian Ocean cooling configuration. The mode accounts for 54% of the squared covariance between West African rainfall and tropical SST anomalies. Sensitivity experiments with two atmospheric general circulation models (AGCMs) are performed to explore the contribution to West African rainfall of SST anomalies corresponding to this mode in different ocean basins.

If SST anomalies are restricted to the Atlantic, the pattern of rainfall anomalies over West Africa forms a north-south dipole, with poles over the Sahel and the Gulf of Guinea. If SST anomalies are taken over the global tropics, however, the pattern becom0es a monopole with center over West Africa, in agreement with the observation after the 1970's. A suggestion from previous studies is therefore demonstrated: After the 1970's, the impacts of SST anomalies in the Atlantic counteract those in the Pacific-Indian Oceans in terms of generating rainfall anomalies over the Sahel.

These results have important implications for the improvement of seasonal forecasts of Sahelian rainfall, and for the better understanding of multidecadal modulations of global interannual teleconnections.

## 1. Introduction

The sea surface temperature (SST) anomaly field has been a key driver of decadal Sahelian rainfall variability during the late 20th century (Folland et al. 1986; Palmer 1986; Rowell et al. 1995; Mohino et al, 2010). Previous studies have focused on the partial impact of the Equatorial Atlantic and Indo Pacific basins on West African precipitation. Tropical Atlantic variability has been related to an anomalous dipole of precipitation with opposite signs over the Sahel and the Gulf of Guinea (Janicot 1992; Shinoda and Kawamura 1994; Rowell et al. 1995; Ward 1998; Janicot et al., 1998; Vizy and Cook, 2002; Paeth and Friederichs, 2004; Nicholson and Webster 2007; Losada et al., 2010a). Several works find negative correlations between the Sahelian rainfall in summer and the tropical Pacific SSTs (Folland et al., 1986; Rowell et al., 1995; Ward 1998; Janicot et al., 1998; 2001; Giannini et al., 2003; Paeth and Friederichs, 2004; Mohino et al., 2011a).

Losada et al. (2010a) have concentrated on the Atlantic, and examined the contribution of SST anomalies restricted to the tropical part of that basin by performing sensitivity experiments with several AGCMs. In that study, the prescribed SST anomalies are based on the inter-annual mode of covariability with West African rainfall after the 1970's as computed by Polo et al. (2008). According to Losada et al. (2010a), such Atlantic SST anomalies result in rainfall anomalies of the same sign over the Gulf of Guinea and of the opposite sign over the Sahel. This dipole-type configuration of rainfall anomalies represents a meridional displacement of the Intertropical Convergence Zone (ITCZ) and the monsoonal flow. Mohino et al. (2011a) have carried out a similar study using observations and several AGCMs, except that SST anomalies are restricted to the Indo-Pacific basin. For the spring season, they have found that a warming (cooling) of the tropical Pacific alters the global Walker circulation leading to decreased (increased) rainfall in the Gulf of Guinea. For the

summer season, a warming (cooling) in the Pacific leads to enhanced (decreased) large-scale subsidence over West Africa, and to decreased (increased) precipitation in the Sahel, which means a weakening (strengthening) of the West African monsoon.

Some studies, however, report that the relation between the SST and the summer rainfall over West Africa involve different oceanic basins depending on the periods of study. In this way, very similar SST anomaly patterns in the Atlantic before and after the 1970's have been related with different patterns of Sahelian rainfall (Janicot et al., 2001; Joly and Voldoire, 2009; Rodriguez-Fonseca et al., 2011; Mohino et al. 2011b, hereafter MO11). Also, the relation between El Niño-Southern Oscillation and Sahelian rainfall seems to be stronger after the 1970's (Trazska et al., 1996; Janicot et al., 1996; 2001).

MO11 investigate the relationship between tropical SSTs and summer Sahelian rainfall – both before and after the 1970's - using observations and an ensemble of five AGCMs. Their results reveal that, after the 1970's, the pattern of rainfall anomalies associated with the Atlantic Niño is no longer of the dipole-type. Instead, a warming (cooling) of SSTs in the Gulf of Guinea appears associated with a monopole-type of positive (negative) rainfall anomalies in West Africa together with weak impacts on the Sahel.

These changes in the correlations of Atlantic SSTs anomalies and West African rainfall take place at about the same time as tropical SST anomalies in the different oceans begin to correlate significantly at interannual time scales (Terray et al. 2005; Terray and Dominiak, 2005; Polo et al., 2008; Rodriguez-Fonseca et al., 2009; Terray 2011). Particularly after the 1970's, Atlantic Niños in the northern summer tend to appear simultaneously with the cold phase of Pacific ENSO events (Polo et al., 2008; Rodriguez-Fonseca et al., 2009, 2011). During this period of time, the variability in the tropical Atlantic and in the Pacific becomes significantly anticorrelated via modifications of the Walker circulation (Wang 2006;

Rodriguez-Fonseca et al., 2009; Losada et al., 2010b; Jansen et al., 2009).

These observational evidences could be interpreted from two different viewpoints, which do not necessarily exclude each other. On the one hand, mechanisms of climate covariability could have changed at the basin level and similar SST anomalies in the Atlantic could have different impacts on West African rainfall. On the other hand, the impact of SST anomalies on West Africa could no longer be examined in a framework restricted to the Atlantic basin and contributions of other oceans should be included in the analysis.

The present paper examines the validity of those two viewpoints. Accordingly, we consider SST anomalies either in single ocean basins or jointly in the global domain both before and after the 1970's. We start in section 2 by contrasting the relationship between atmospheric and SST anomalies before and after the 1970s on the basis of observational data. Section 3 introduces the global mode of co-variability between SSTs and West African rainfall. Section 4 describes selected results of our AGCM sensitivity experiments. Sections 5 presents summary of those results, and outlines the main conclusions of the study.

## 2. Contrasting the relationship between atmospheric and SST anomalies before and after the 1970s

Our first concern in this section is to identify, for the three ocean basins, the time sequences of SST anomalies in the tropics that co-vary with rainfall anomalies over West Africa. Here West Africa (hereafter WA) is defined as the region between 21.25W-33.75E, 6.25S-31.25N. As in MO11, the three SST modes are obtained by application of an Extended Maximum Covariance Analysis (EMCA) in a similar way than in Polo et al. (2008). The predictor field consists of the SST anomalies during four-month sequences starting in the sequence from February to May (FMAM) and ending in the one from September to December (SOND). The predictand field is the precipitation over WA in the sequence from June to September (JJAS).

We apply the EMCA separately for the periods 1957-1978 and 1979-1998. We choose these periods for two reasons: first, to be consistent with MO11 work. Second, to be able to use satellite-based rainfall data, which is available from 1979 onwards and provides spatial continuity, covering both the continent and the ocean.

Next, we regress in the global domain both the SST and atmospheric fields (represented by the velocity potential at 200 hPa) onto the expansion coefficient of the SST (SST-EC) for the leading EMCA modes computed *separately* for the three ocean basins and the two time periods considered. Our datasets are the monthly-mean precipitation from the CPC Merged Analysis of Precipitation (CMAP, Xie and Arkin, 1997) and Climate Research Unit (CRU, UK, Hulme, 1992), Reynolds Reconstructed SST data (Smith and Reynolds, 2004), and ERA40 reanalysis (Uppala et al., 2005).

Starting with the SST, Figure 1 shows the regressions of this field onto the SST-EC for the leading EMCA modes of tropical SST in the three basins and WA rainfall for both the 1957-1978 and 1979-1998 periods (left and right columns, respectively). In the former period, the regressions show very small values outside the ocean basin for which the ECMA mode was computed. In the latter period the situation is a very different one. The global SST field regressed onto the individual ocean SST-EC shows in all three cases an El Niño-like pattern in the Pacific, together with La Niña-like conditions in the tropical Atlantic (see also Rodriguez-Fonseca et al. 2009; Polo et al. 2008, and MO11). The global patterns also show some similarities in the extra-tropics, which could be related to the tropical forcing of extra-tropical SSTs, the tropical-extra-tropical interaction is beyond the scope of this study.

We next turn to the atmosphere in Figure 2, which shows a regression of the velocity potential at 200 hPa onto the SST-EC of the different EMCA analyses. The pattern corresponding to the tropical Pacific SST-WA rainfall mode captures a Southern Oscillation

configuration for both periods (Figure 2 a-b), reflecting changes in the Walker circulation over the Pacific. The centers of action are slightly nearer the equator in the 1979-1998 period. Such a feature may be due to the simultaneous warming over the western Indian and cooling of the Equatorial Atlantic during that period. Regression on the SST-EC of the Atlantic SST-WA rainfall mode has small values in the Pacific in the 1957-1978 period (Figure 2c), while it captures again a Southern Oscillation-like pattern in the Pacific in the 1979-1998 period (Figure 2d). A similar situation is obtained regressing the velocity potential at 200 hPa onto the principal component of the tropical Indian Ocean SST-WA rainfall mode (Figure 2e-f).

According to Figures 1 and 2, therefore, in the 1957-1978 period there is little resemblance between the three regression patterns, which have very small values outside the reference basin. In the 1979-1998 period, the global signature of each of the tropical basins leading modes correspond to a similar global tropical pattern, including the influence of the Atlantic, Pacific and Indian oceans. Also for this period, there is a unique atmospheric response to the Atlantic, Pacific and Indian SST leading modes, resulting in a Southern Oscillation signal whose action centers span the global equatorial band.

**3 The Global Tropical SST mode in reference to WA rainfall**

In view of the results presented in section 2 of this paper, we apply the EMCA to the anomalies in SST over the global tropics (in the region between 180W-180E, 20S-20N) and WA rainfall for the periods 1957-1978 and 1979-1998 using CRU data. For 1979-1998 we also compute the EMCA analysis using CMAP data. For the second period, results of both analyses are robust and highly consistent. To be concise, we will only show the results of the EMCA analysis performed with CMAP data, which also covers oceanic regions.

The results of the EMCA for the 1957-1978 period are not statistically significant (Rodríguez-Fonseca et al., 2011). Conversely, the results for the 1979-1998 period (Figure 3)

are robust and account for 54% of the squared covariance fraction (scf) between West African rainfall and SST anomalies in the tropical oceans. The correlation between expansion coefficients of SST and precipitation anomalies is very high (ruv=73%). To assess the robustness of this analysis we perform a Monte Carlo test to the scf and ruv. We shuffle the data and apply the EMCA 100 times. The probability density functions of scf and ruv parameters from the random realizations are compared with the non-shuffled scf and ruv scores (Figures 3j and 3k), showing that both scf and ruv are robust and significant. The EMCA analyses performed with CRU data produce similar results, accounting for 71% of scf and with ruv=64% (Rodríguez-Fonseca et al., 2011). The high percentage of WA rainfall variability explained by this mode could have strong applications in seasonal predictability of Sahelian rainfall.

According to Figure 3, the leading precipitation pattern in the four-month sequence June-September is primarily a one-signed structure over the whole WA region with maximum loadings over the Gulf of Guinea. Nevertheless, there is a clear seasonal evolution of the anomalous rainfall. For negative lags, the pattern of precipitation anomalies shows a dipolar structure, with positive values over the Gulf of Guinea for the warm Atlantic (cold Pacific) phase of the mode. For positive lags, the structure is one-signed over the whole WA. The northward displacement of the precipitation anomalies from June-September onwards is in agreement with the seasonal cycle of the ITCZ.

Regarding the SST pattern, maximum loadings are shown in the four-month sequence February-May over the eastern equatorial Pacific basin and over the southeastern tropical Atlantic, with different signs over the tropical Atlantic and Pacific. Also, some SST anomalies appear over the western Indian Ocean from March-July, with the same sign of those in the eastern Pacific. During the following months, the signal over the Atlantic evolves

from the Angola-Benguela upwelling region towards the Equator, presenting maximum amplitudes in May-August. From June-September the Atlantic SST anomalies decay until September-December, when there are no significant anomalies over the tropical Atlantic. This evolution of SST anomalies is in agreement with the one described in the observational analysis of Polo et al. (2008) and the pattern used in Losada et al (2010a, 2010b) for their AGCM experiments. Over the tropical Pacific, a Niño-like pattern with anomalies of opposite sign than those of the tropical Atlantic is apparent during the whole sequence. As the season advances, the maximum loadings over the eastern Pacific extend westward and cover a wider latitudinal band, while the anomalies over the Maritime Continent become more important.

## 4. Effects of the Global Tropical SST Mode on WA rainfall

### *4.1 Experimental set up*

This section presents the results from AGCM sensitivity experiments aimed to gain dynamical insight on the relationship between tropical SST anomalies and WA precipitation. We use UCLA v.7.3 (Mechoso et al., 2000; Richter et al. 2008) and LMDZ v.4 (Hourdin et al. 2006) AGCMs, which are the only models in MO11 that show a significant correlation between simulated and observed interannual variability in Sahelian rainfall. The experiments consist of seven-month long integrations from March through September.

To produce the monthly-mean boundary conditions in SST anomalies for the AGCM experiments we choose the years during the period 1979-1998 in which the absolute value of the June to September SST-EC of the global mode is larger than one standard deviation in at least 2 out of the 4 months, and the June to September precipitation expansion coefficient has the same sign as that of the SST for at least 3 of those months. This gives three years with negative expansion coefficients (1982, 1983, 1997 or “negative years”) and four years with

positive expansion coefficients (1985, 1988, 1989, and 1996 or "positive years"). The SST anomalies for the AGCM experiments are defined as the difference between the fields for the positive and negative years. To test the statistical significance of the composite analysis we perform a Monte Carlo test: a random selection of years with positive an negative SST-EC is performed 100 times, giving 100 "positive minus negative" composite maps. Then the non-shuffled "positive minus negative" map is compared with the 100 random "positive minus negative" permutations, obtaining a confidence level for the anomalies.

The resulting SST fields and corresponding observed rainfall anomalies are presented in Figure 4. From March to June, the anomalous rainfall conforms an anomalous dipolar precipitation pattern, with increased precipitation over the Gulf of Guinea and decreased precipitation to the north. At the end of summer (July and August) the anomalies in the Atlantic weaken, those in the Pacific widen, and those around the Maritime Continent strengthen, the anomalous precipitation dipole disappears over West Africa, and positive rainfall anomalies cover the Sahel and Gulf of Guinea.

We perform three sensitivity experiments in which the SST anomalies shown in Figure 4 are either partially or fully added to the mean SST values for the 1979-2005 period: 1) "GM experiment", in which the SST anomalies are those in Figure 4; 2) "TA experiment", in which only the SST anomalies in the Tropical Atlantic are retained, and 3) "IP experiment", which is similar to TA, except that the anomalies retained are those in the Indian and Pacific Oceans. The Indian and Pacific Ocean are taken together because the EMCA between Indian SST and WA rainfall is non-robust (see MO11) and, although the Indian Ocean has its own variability, the variability of the SSTs over the Maritime Continent is highly coupled to the Pacific Ocean. To avoid discontinuities in the SST field, the anomalies decrease linearly in the four grid points polewards of 30N and 30S. Note that the years chosen for the composite

of the TA experiment are different from those in Losada et al. (2010a), which gives a different anomalous SST pattern with smaller amplitudes. Also note that there are several important differences between the SST anomaly fields in the IP experiment and the ones performed used in Mohino et al. (2011a). First, values over the western Indian Ocean are stronger in IP. Second, values around the Maritime Continent are also stronger in IP and extend further west to achieve maximum amplitudes during the monsoon peak.

For each AGCM, the sensitivity experiments consists of 10-member ensemble integrations, in which ensemble members differ in a slight perturbation of the initial conditions. The control simulation consists also of one ten-member ensemble integrations with climatological, monthly-mean varying SST corresponding to the 1979-2005 period. To evaluate the atmospheric response to the anomalous SSTs, we calculate the difference between the multi-model ensemble mean of the sensitivity experiments and the control simulation following Krishnamurti et al. (2000a, b). We also identify the areas of high consistency between models as those where the amplitude of the multi-model mean is larger that the inter-model standard deviation (Meehl et al., 2007; Mohino et al., 2011a).

*4.2 Results and mechanisms*

Figure 5 shows the simulated monthly-mean precipitation anomalies from May to August, obtained in the TA, IP and GM experiments. In TA, the precipitation response to a *warming* in the tropical Atlantic (Figure 5a-d) shows a dipolar pattern, with positive rainfall anomalies over the Gulf of Guinea and negative ones to the north reaching 15N. Magnitudes are larger in spring (May-June), when SST anomalies are strong. In IP, the precipitation response during spring (May and June) to a *cooling* of the eastern Pacific (Figure 5e-h) shows the northward displacement of enhanced precipitation from the Gulf of Guinea to the Sahel as the season advances. Finally, in GM, precipitation anomalies of (Figure 5j-l) resemble the

observed ones (Figure 4), with a dipolar structure before the monsoon onset that disappears during the monsoon season, when they present a more monopolar configuration. The results of TA and IP are similar those obtained by Losada et al. (2010a) and Mohino et al. (2011a), respectively.

The dynamical mechanisms at work in the TA experiment are similar to those described in Losada et al. (2010a). These include changes in the large-scale circulation induced by the reduction of the surface pressure gradient by the tropical Atlantic warming (not shown). The results obtained here, therefore, confirm that those of Losada et al. (2010a) were not due to the amplification of the SST anomalies prescribed in their AGCMs.

Figure 6 shows height-latitude cross-sections, averaged between 10W-10E, of the May-August monthly anomalous horizontal moisture flux divergence from the TA experiment. Our results capture an enhancement of the moisture convergence in the boundary layer along the Gulf of Guinea, consistent with an increase of the evaporation in the tropical Atlantic. There is also moisture convergence in the middle troposphere. From July on, the convergence center is located over the southern Sahel where precipitation decreases (Figure 5c-d) and sinking motion increases in the middle troposphere (not shown). From these results one can conclude that for a warming in the Equatorial Atlantic the increase of moisture flux convergence causes the enhancement of the precipitation over the Gulf of Guinea, which is in agreement with previous studies (Bader and Latif, 2011). Nevertheless, the latitudinal extension of the anomalies, and the presence of negative anomalies over the Sahel, is primarily determined by the large-scale circulation (see also Losada et al. 2010).

Figure 5a-d also shows negative precipitation anomalies over central Africa and a strong east-west rainfall dipole in July and August. Such anomalies could be a response to the anomalous diabatic heat source located over the coast of Guinea, which produces a surface flow directed

to the heat source and a modification of the Walker circulation over Africa.

In the IP experiment, the cooling of the eastern Pacific and western Indian Oceans, together with the warming of the ocean around Maritime Continent lead to an increase in precipitation over the Gulf of Guinea in May and June (Figure 5e-f), followed by an enhancement of the Sahelian rainfall during July and August (Figure 5g-h), in agreement with Mohino et al. (2011a). To examine the upper level circulation associated with the Indo-Pacific forcing, we analyze the monthly-mean anomalies of the eddy-streamfunction at 200 hPa (Figure 7), and the anomalous divergent circulation at the same level (Figure 8). The eddy-streamfunction is defined as the deviation from the zonal mean. In May, a pair of anomalous cyclones straddling the equator covers the equatorial Pacific, consistent with a Gill-Matsuno response to an equatorial diabatic cooling (Gill, 1980) in the region. At this stage, an anomalous cyclonic circulation covers the whole tropical Pacific. Also, two pairs of anomalous anticyclones appear at both sides of the equator in the Indian (70E) and Atlantic (20W). The former is consistent with an equatorial Rossby wave response to the warming over the Indian Ocean; while the latter pair could be the response to the anomalous tropospheric warming associated with increased convection over the tropical Atlantic, due to the modification of the Walker circulation by the cooling in the eastern Pacific. This global response, which basically extends till June, also includes anomalous divergence over the equatorial Atlantic (Figure 8), with enhanced ascending motions and precipitation over the Gulf of Guinea, together with a decrease in the rainfall to the north.

During July and August, the anomalous anticyclones over the equatorial Atlantic at upper levels are confined to the western part of the basin, coherently with the westward propagation of the SST anomalies in the Pacific (Figure 7 c-d). From July on, the West African region appears to be more influenced by anomalous circulation features propagating from the Indian

region. The anomalous SST pattern in July and August (Figure 4e-f) presents an intensification of the warming over the Maritime Continent with respect to May and June (Figure 4c-d), producing the enhancement of the anomalous upper level divergence there (Figure 8, c-d). The cooling of the western Indian Ocean and, thus, the anomalous upper level convergence there is maintained. These features produce the intensification of the anomalous anticyclonic circulation over India in August, which affects the circulation over the African continent (Figure 7d). During the same month, in the Southern Hemisphere, extratropical Rossby waves are excited from the Pacific and propagate to the Atlantic sector, which intensifies the South Atlantic anticyclone, extending downstream the eastern tropical south Atlantic and the African continent (Figure 7d). This anomalous configuration is consistent with a region of upper level anomalous convergence centered over the African continent around the equator (Figure 8d). Although this feature is much more intense in August, it is also present in July, and produces an anomalous divergence in the Sahel, responsible for the anomalous precipitation pattern in Figure 5g-h. The results basically agree with those of Mohino et al. (2011a), despite some differences in the large-scale patterns due to the different SST anomalous patterns used in both works.

Finally, the monthly anomalous eddy-streamfunction and wind divergence at 200 hPa obtained in the GM experiment are displayed in Figures 9 and 10, respectively. In May and June, the eddy-streamfunction pattern is very similar to the one in IP, although the anomalous circulation over the Atlantic is stronger, and the one over the Indian sector is weaker. This is consistent with the large-scale effect of the tropical Atlantic warming described in Kucharski et al. (2009) and Losada et al. (2010b). That is, diabatic heating over the tropical Atlantic produces a Gill-Matsuno type response with anomalous subsidence over the Indian sector. In the GM experiment, the latter counteracts the Gill response to the warming of the Maritime

Continent, leading to the weakening of the anomalous anticyclone there (Figure 9c-d). During this month, the Atlantic and IndoPacific SST anomalies have a similar impact on West African precipitation when acting separately (Figure 5a-b, e-f). Thus, one would expect that the joint action of these anomalies would interact constructively in terms of anomalous precipitation in May and June. Figure 5i-j confirms this hypothesis, highlighting the linearity of the response.

In July and August, the warm Atlantic SSTs continue to produce the enhancement of the local upper level divergence, and the weakening of the upper level anticyclone and the anomalous ascendant motions and the 200 hPa divergence over the Indian sector (Losada et al., 2010b; Kucharski et al., 2009). The effect of TA SSTs on the large-scale circulation over the Indian sector is opposite to that of IP SSTs. Therefore, the combined action of these circulation anomalies leads to the disappearance of the maximum anomalous convergence over equatorial Africa that appeared in IP. With this anomalous pattern in the upper troposphere, there is upper level divergence from the Sahel to the equatorial Atlantic (Figure 10c-d), producing the enhancement of the precipitation over the Gulf of Guinea and the Sahel during August.

The anomalous circulation patterns in the GM experiment are approximately the sum of those in TA and IP (Figure 11). For May and June, the Atlantic warming and the Pacific cooling would add their effects in the Equatorial Atlantic, increasing the surface convergence and retaining the ITCZ to the south and resulting in the anomalous rainfall dipole. From July on, the SST anomalies of the Equatorial Atlantic extend west and weaken greatly, leading to the weakening of the anomalous dipole. During this month, the maximum SST anomalies over the Pacific widen and the moisture convergence in the Atlantic is displaced northward, tied to the seasonal cycle. The influence of the Indian and western Pacific SST becomes dominant

over the Sahel, increasing the upper level divergence over this region and counteracting the effect of the Atlantic, leading to the disappearance of the anomalous rainfall dipole and favoring the development of positive rainfall anomalies over the Sahel, that would produce a monopolar rainfall pattern over WA in August.

**5. Discussion and conclusions**

This paper re-examines in a global context the relationships between WA rainfall variability and tropical SSTs addresses in previous works primarily performed in a basin-context (Joly and Voldoire 2010; Rodriguez-Fonseca et al., 2011; MO11). MO11 find that the interannual rainfall variability could be modulated by multidecadal relationships that exist between the Atlantic and the Pacific oceans after the 1970's. We find that the modulation is established through a global mode of covariability between rainfall and SST in that period. Next we examine how the existence of such a mode makes the relationships to be non-stationary and requires the problem be addressed in the global context

Before the 1970's, the patterns of co-variability between WA rainfall and SST anomalies in each of the tropical ocean basins have insignificant projections outside the basin considered. On the contrary, after the 1970's, the global projections of these patterns show significant values in all the basins, with a similar spatial configuration. We find that after the 1970's all the tropical ocean basins conform a leading robust mode of SST in relation to WA rainfall variability. This global mode accounts for 54% of the squared covariance, and it is defined as a time-evolving SST-rainfall pattern that can be described as a "Pacific Niña, Atlantic Niño and cooling of the western Indian Ocean" (and the opposite) in relation to an increase (reduction) of rainfall in WA.

We demonstrate that in such a framework of inter-basin relationships that takes place during the 1979-1998 period, one should consider the SST anomalies in the global tropics in order to

properly portray their influence on Sahelian rainfall. Our methodology is based on performing three different sensitivity experiments with two AGCMs. In the experiments, we add to the climatological SST anomalous pattern corresponding to either the global mode (GM), or the Atlantic (TA) and the Indo-Pacific (IP) components, separately.

Results of TA and IP experiments are in agreement with previous findings about the WA rainfall response to tropical Atlantic SST anomalies (Losada et al., 2010a; Bader and Latif, 2011), and to tropical Indo Pacific anomalies (Mohino et al., 2011a).

The anomalous pattern of WA precipitation simulated in the GM experiment closely resembles that of the observations. This coincidence is supportive of the hypothesis on the Atlantic-Pacific influence on the West African Monsoon stated in previous works (Joly and Voldoire, 2010; Rodríguez-Fonseca et al., 2011; MO11). The combined impact of the SST anomalies on the equatorial Atlantic, Pacific and Indian oceans on WA rainfall after the 1970's is a key contributor to the disappearance in summer of the anomalous rainfall dipole described as a response to SST anomalies in the equatorial Atlantic. In spring (June and May), the SST anomalies in the tropical Atlantic would produce a dipole of anomalous precipitation over WA. At this stage the SST anomalies in the IndoPacific would produce a similar although weaker dipole of anomalous rainfall in WA, reinforcing the impact of the SST anomalies in tropical Atlantic over WA. In summer (July and August), the influence of the SST anomalies in the IndoPacific over the Sahel is opposite to that of the SST anomalies in the tropical Atlantic. This counteracting effect produces the weakening and disappearance of the dipolar feature of WA precipitation in July and August.

The mechanisms presented in this paper are related to equatorial dynamics involving different Gill-Matsuno responses to anomalous diabatic cooling or heating in each of the tropical basins. The response is highly linear in the tropics, and the influence of each basin

can be added to the rest of them to produce an upper tropospheric signal in the tropical regions similar to the observed one.

These findings provide an explanation for two features described for the after-1970's period in WA during summer: 1) the lack of significant negative correlation between precipitation anomalies in the Gulf of Guinea and the Sahel (Polo et al., 2008; Joly and Voldoire, 2010); and 2) the disappearance of the precipitation anomalies of opposite sign over the Sahel and the Gulf of Guinea in response to tropical Atlantic SST anomalies in summer (MO11). They also confirm previous hypothesis about the counteracting effect of Pacific and Atlantic SST on Sahel rainfall during the post-1970's period (Joly and Voldoire, 2010; MO11), thus providing an explanation for the multidecadal modulation of the correlation between Guinean Gulf and Sahelian precipitation anomalies.

According to our results, the impact of the individual ocean basins on WA rainfall seems to be relatively stable over time and first order stationary. This is demonstrated e.g by the TA experiment which clearly produces a rainfall dipole pattern in summer over WA. The bottom line is that the covariability of the SSTs in the tropical Atlantic and other tropical basins is non-stationary. Before the 1970, the SST anomalies in the tropical Atlantic are fundamentally uncorrelated with those elsewhere, whereas after the 1970's they appear in combination with others in the Indian and Pacific oceans. The constructive and desstructive interferences among SSTs results in significant changes of anomalous precipitation patter over WA.

This result opens important discussions regarding the origin of the multidecadal modulation of the interannual modes of SST, as well as about its implications on the non-stationary behavior of Sahelian precipitation. Such modulation could be related to changes in the background state, due to multidecadal variability of SST (Dong et al., 2006; Mohino et al., 2010). In agreement with Joly and Voldoire (2010), figure 12 shows that correlations between

Niño3 index (defined as the SST anomaly in the region 5ºS-5ºN, 150ºW-90ºW) and precipitation in the Gulf of Guinea, as well as those with precipitation in the Sahel, are significant for the post-1970's pre-1920's periods. The relation between Guinean Gulf rainfall and the ATL3 index (defined as the SST anomaly in the region 3ºS-3ºN; 20ºW-0ºE) is stationary along the 20th century; conversely, the negative correlation between Sahel precipitation and ATL3 is significant only during the period between 1920-1970, when the dipole of anomalous rainfall appears. According to our results, this behavior of the correlations is due to changes in the background state acting as modulator of the interannual Pacific-Atlantic connection and its impact on WAM rainfall, affecting the correlations between precipitation in West Africa (GG and Sahel) and Pacific and Atlantic SST anomalies at multidecadal time scales. We are currently investigating the mechanisms at work for the influence of the background state on the interannual variability of tropical rainfall.

**Acknowledgments**

This project has been partially funded by the EU-AMMA project. Based on French initiative, AMMA was built by an international scientific group and is currently funded by a large number of agencies, especially from France, UK, US and Africa. It has been the beneficiary of a major financial contribution from the European Community's Sixth Framework Research Programme. Detailed information on scientific coordination and funding is available on the AMMA International website http://www.amma-international.org. This study has been also supported by the Spanish projects: MICINN CGL2009-10285, MMA MOVAC-200800050084028 and the Research Group "Micrometeorology and Climate Variability". We would like to thank the EEA 'Abel extraordinary chairs' for the mobility grant of Dr Rodriguez-Fonseca to the Bjerknes Center for Climate Reasearch and the University of Bergen. The research at UCLA was funded by NSF grant AGS-1041477.

**References**

Bader, J., and M. Latif, 2003: The impact of decadal scale Indian ocean SST anomalies on Sahelian rainfall and the North Atlantic Oscillation. *Geophys. Res. Lett.*, **30**, 2169. Doi:10.1029/2003GL018426.

Bader, J., and M. Latif, 2011: The 1983 drought in the West Sahel: a case study. *Clim. Dyn*., **36**, 463-472. DOI: 10.1007/s00382-009-0700-y.

Dong, B.-W., R.T. Sutton, and A. A. Scaife, 2006: Multidecadal modulation of El Niño-Southern Oscillation (ENSO) variance by Atlantic Ocean sea surface temperatures. *Geophys. Res. Lett.*, **33**, L08705, doi:10.1029/2006GL025766.

Folland, C.K., T.N. Palmer, and D.E. Parker, 1986: Sahel rainfall and worldwide sea temperatures, 1901−85. *Nature*, **320**, 602-607, Doi:10.1038/320602a0.

Giannini, A., R. Saravannan, and P. Chang, 2003: Oceanic forcing of Sahel rainfall on interannual to interdecadal time scales. *Science*, **302**, 1027–1030.

Gill, A.E., 1980: Some simple solutions for heat-induced tropical circulation. *Quat. J. R. Met. Soc.*, **106**, 447-462.

Hourdin, F., I. Musat, S. Bony, P. Braconnot, F. Codron, J.L. Dufresne, L. Fairhead, M.A. Filiberti, P. Friedlingstein, J.Y. Grandpeix, G. Krinner, P. LeVan, Z.X. Li, F. Lott, 2006: The LMDZ4 general circulation model: climate performance and sensitivity to parametrized physics with emphasis on tropical convection. *Clim. Dyn*., **27**, 787–813.

Hulme, M., 1992: A 1951-80 global land precipitation climatology for the evaluation of general circulation models. *Clim. Dyn*., **7**, 57-72.

Janicot, S., 1992: Spatiotemporal variability of West African rainfall. Part II: associated surface and airmass characteristics. *J. Clim.*, **5**, 499–511.

Janicot, S., A. Harzallah, B. Fontaine, and V. Moron, 1998: West African monsoon dynamics and eastern equatorial Atlantic and Pacific SST anomalies (1970–1988). *J. Clim.*, **11**, 1874–1882.

Janicot, S., V. Moron, and B. Fontaine, 1996: ENSO dynamics and Sahel droughts. *Geophys. Res. Lett.*, **23**, 515–518.

Janicot, S., S. Trzaska, and I. Poccard, 2001: Summer Sahel-ENSO teleconnection and decadal time scale SST variations. *Clim. Dyn*., **18**, 303-320.

Jansen, M.F., D. Dommenget, and N. Keenlyside, 2009: Tropical Atmosphere–Ocean Interactions in a Conceptual Framework. *J. Climate*, **22**, 550–567.

Joly, M., and A. Voldoire, 2009: Influence of ENSO on the West African Monsoon: Temporal Aspects and Atmospheric Processes. *J. Climate*, 22, 3193–3210.

Joly, M., and A. Voldoire, 2010: Role of the Gulf of Guinea in the inter-annual variability of the West African monsoon: what do we learn from CMIP3 coupled simulations?. *International Journal of Climatology*, **30**, 1843–1856. doi: 10.1002/joc.2026.

Krishnamurti, T.N., C.M. Kishtawal, Z. Zhang, T. LaRow, D. Bachiochi, E. Williford, S. Gadgil, and S. Surendran, 2000a: Multimodel ensemble forecasts for weather and seasonal climate. *J. Climate*, **13**, 4196-4216.

Krishnamurti, T.N., C.M. Kishtawal, D.W. Shin, and C.E Williford., 2000b: Improving tropical precipitation forecasts from a multianalysis superensemble. *J. Climate*, **13**, 4217-4227.

Kucharski, F., A. Bracco, J. H. Yoo, A. Tompkins, L. Feudale, P. Ruti, and A. Dell'Aquila, 2009: A Gill-Matsun-type mechanism explains the Tropical Atlantic influence on African and Indian Monsoon Rainfall. *Quart. J. R. Met. Soc.*, **135**, 569-579.

Losada, T., B. Rodriguez-Fonseca, S. Janicot, S. Gervois, F. Chauvin, and P. Ruti, 2010a: A multimodel approach to the Atlantic ecuatorial mode. Impact on the West African monsoon. *Clim. Dyn.*, Doi: 10.1007/s00382-009-0625-5.

Losada, T., B. Rodriguez-Fonseca, I. Polo, S. Janicot, S. Gervois, F. Chauvin, and P. Ruti, 2010b: Tropical response to the Atlantic Equatorial mode: AGCM multimodel approach. *Clim. Dyn*., Doi: 10.1007/s00382-009-0624-6.

Mechoso, C.R., J.Y. Yu, A. Arakawa, 2000: A coupled GCM pilgrimage: from climate catastrophe to ENSO simulations. In: Randall DA (ed) General Circulation Model Development: past, present and future. Proceedings of a symposium in honor of Professor Akio Arakawa. Academic, New York, pp 539–575

Meehl, G. A., F. S. Thomas, W. D. Collins, P. Friedlingstein, A. T. Gaye, J. M. Gregory, A. Kitoh, R. Knutti, J. M. Murphy, A. Noda, S. C. B. Raper, I. G. Watterson, A. J. Weaver, and Z. C. Zhao, 2007: Global climate projections. *Climate Change 2007: The Physical Science Basis. Contribution of Working Group I to the Fourth Assessment Report of the Intergovernmental Panel on Climate Change.* S. Solomon, D. Qin, M. Manning, Z. Chen, M. Marquis, K. B. Averyt, M. Tignor, and H. L. Miller, Eds., Cambridge University

Mohino, E., S. Janicot, and J. Bader, 2010: Sahel rainfall and decadal to multi-decadal sea surface temperature variability. *Clim. Dyn*., Doi: 10.1009/s00382-010-0867-2.

Mohino, E., B. Rodríguez-Fonseca, C.R. Mechoso, S. Gervois, P. Ruti, and F. Chauvin, 2011a: Impacts of the Tropical Pacific/Indian Oceans on the Seasonal Cycle of the West African Monsoon. *J. Clim.,* Doi: 10.1175/2011JCLI3988.1.

Mohino, E., B. Rodríguez-Fonseca, T. Losada, S. Gervois, S. Janicot, J. Bader, P. Ruti and F. Chauvin, 2011b: SST-forced signals on West African rainfall from AGCM simulations-Part I: changes in the interannual modes and modelintercomparison. *Clim. Dyn*., Doi: 10.1007/s00382-011-1093-2.

Nicholson, S.E., and P.J. Webster, 2007: A physical basis for the interannual variability of rainfall in the Sahel. *Quart. J. R. Met. Soc.*, **133**, 2065–2084. doi:10.1002/qj.104.

Paeth, H., and P. Friederichs, 2004: Seasonality and time scales in the relationship between global SST and African rainfall. *Clim. Dyn.*, **23**, 815–837. doi:10.1007/s00382-004-0466-1.

Palmer, T.N., 1986: Influence of the Atlantic, Pacific and Indian Oceans on Sahel rainfall. *Nature*, **322**, 251-253. Doi:10.1038/322251a0.

Polo I., B. Rodríguez-Fonseca, T. Losada, and J. García-Serrano, 2008: Tropical Atlantic Variability modes (1979-2002). Part I: time-evolving SST modes related to West African rainfall. *J. Climate*, **21**, 6457–6475. Doi: 10.1175/2008JCLI2607.1.

Richter, I., C.R. Mechoso, A.W. Robertson, 2008: What determines the position and intensity of the south Atlantic anticyclone in Austral Winter? An AGCM study. *J. Clim.*, **21**, 214–229.

Rodríguez-Fonseca, B., I. Polo, J. García-Serrano, T. Losada, E. Mohino, C. R. Mechoso, and F. Kucharski, 2009: Are Atlantic Niños enhancing Pacific ENSO events in recent decades?, *Geophys. Res. Lett.,* **36**, L20705, Doi:10.1029/2009GL040048.

Rodríguez-Fonseca, B., S. Janicot, E. Mohino, T. Losada, J. Bader, C. Caminade, F. Chauvin, B. Fontaine, J. García-Serrano, S. Gervois, M. Joly, I. Polo, P. Ruti, P. Roucou, and A. Voldoire, 2011: Interannual and decadal SST forced responses of the West African monsoon. *Atmos. Sci. Lett*., **12**, 67-74. Doi: 10.1002/ASL.308.

Rowell, D.P., C.K. Folland, K. Maskel, J.A. Owen, and M.N. Ward, 1995: Variability of the summer rainfall over tropical North Africa (1906-92): Observations and modeling. *Quat. J. Roy. Meteor. Soc.*, **121**, 669-704. Doi: 10.1002/qj.49712152311.

Shinoda, M., and R. Kawamura, 1994: Tropical rainbelt, circulation and sea surface temperatures associated with the Sahelian rainfall trend. *J. Meteor. Soc. Jpn.*, **72,** 341–357.

Smith, T.M., and R.W. Reynolds, 2004: Imporved Extended Reconstruction of SST (1854-1997). *J. Climate*, **17**, 2466-2477.

Terray, P., and S. Dominiak, 2005: Indian Ocean Sea Surface Temperature and El Niño–Southern Oscillation: A New Perspective. *J. Climate*, 18, 1351–1368.

Terray, P., E. Guilyardi, A.S. Fisher and P. Delecluse, 2005: Dynamics of the Indian monsoon and ENSO relationships in the SINTEX global coupled model. *Clim. Dyn.*, **24**, 145-168.

Terray, P., 2011: Southern Hemisphere extra-tropical forcing: a new paradigm for El Niño-Southern Oscillation. Clim. Dyn., **36**, , 2171-2199, Doi: 10.1007/s00382-010-0825-z

Trzaska, S., V. Moron, and B. Fontaine, 1996: Global atmospheric response to specific linear combinations of the main SST modes. Part I: Numerical experiments and preliminary results. *Ann. Geophys.*, **14**, 1066–1077.

Uppala, S.M. et al., 2005: The ERA-40 Reanalysis. *Quat. J. Roy. Meteor. Soc.,* **131**, 2961-3012. Doi:10.1256/gj04176.

Vizy, E.K., and K.H. Cook, 2002: Development and application of a mesoscale climate model for the tropics: influence of sea surface temperature anomalies on the West African monsoon. *J. Geophys. Res. Atmos.*, **107**, 4023. Doi: 10.1029/2001JD000686.

Wang, C., 2006: An overlooked feature of tropical climate: Inter-Pacific-Atlantic variability. *Geophys. Res. Lett.,* **33**, L12702, Doi: 10.1029/2006GL026324.

Ward, M.N., 1998: Diagnosis and short-lead time prediction of summer rainfall in tropical North Africa at interannual and multidecadal timescales. *J. Clim.*, **11**, 3167–3191.

Wilks, D.S., 2005: Statistical Methods in the Atmospheric Sciences. *Academic Press*, 648 pp. ISBN-13: 978-0-12-75196.

Xie, P., and P.A. Arkin, 1997: Global precipitation: A 17-year monthly analysis based on gauge observations, satellite estimates, and numerical model outputs. *Bull. Amer. Meteor. Soc.*, **78**, 2539–2558.

**Figure Captions:**

**Figure 1:** Observed global SST anomalies (C) regressed onto the SST-EC of the leading mode of the EMCA between June-September (JJAS) precipitation over WA and February-May (FMAM) to September-December (SOND) SST anomalies in the Pacific (first row), Atlantic (second row) and Indian (third row) basins. The first column represents the analysis for 1957-78, the second column represented the analysis for 1979-98. Shading denote 95% statistical significant areas, evaluated with a T-test.

**Figure 2:** Same as Figure 1 but for the 200 hPa Velocity Potential anomalies ($m^2/s$).

**Figure 3: a) to h)** Leading EMCA mode of variability between the February-May (FMAM) to September-December (SOND) global tropical SST anomalies (Reynolds dataset) and June-September (JJAS) WA precipitation (CMAP dataset), in terms of regression maps of the observed SST (C) and precipitation (standardized) anomalies onto the SST expansion coefficient. The Figure presents the homogeneous regression map for the SST (contours; solid (dashed) lines denote positive (negative) SST anomalies) and heterogeneous regression map, lagged over the different time-sequences of the anomalous rainfall (shaded). Only those areas with 95% significant regressions evaluated with a T-test are shown. The results are obtained with ERST SST Data for the SST and CMAP data for the rainfall. **i)** Expansion coefficients of SST (bars) and precipitation (red line) for the leading EMCA mode of variability. **j)** Probability distribution function (pdf) of scf scores derived from a Monte Carlo test with 100 realizations, represented together with the non-shuffled EMCA score (red line). **k)** Same as j) but for ruv score.

**Figure 4:** Composite maps of the observed monthly (from March to August) anomalous rainfall (shaded) and SST (contours; red (blue) lines denote positive (negative) SST anomalies, contour interval is 0.5 C) for the leading global EMCA mode of Figure 3a (cold Pacific and warm Atlantic phase). Dark gray contours denote areas where precipitation is 95% statistically significant with a Monte Carlo test of 100 realizations.

**Figure 5:** May to August monthly-mean anomalies of precipitation (mm/day) a-d) for TA, e-f) IP and i-j) GM experiments. Only those areas where the multimodel ensemble mean is larger in magnitude than the inter-model standard deviation are showed.

**Figure 6:** May to August height-latitude cross-section of the horizontal moisture divergence monthly-mean anomalies (gr/kg·s), averaged between 10W-10E, for TA experiment. Shaded

areas denote those regions where the multimodel ensemble mean is larger in magnitude than the inter-model standard deviation; solid (dashed) lines denote positive (negative) anomalies.

**Figure 7:** May to August 200 hPa eddy-streamfunction monthly-mean anomalies ($10^6$ $m^2s^{-1}$) for IP experiment. Black contours denote those regions where the multimodel ensemble mean is larger in magnitude than the inter-model standard deviation.

**Figure 8:** May to August 200 hPa divergent wind anomalies (m/s) for IP experiment. Black arrows denote those regions where the multimodel ensemble mean is larger in magnitude than the inter-model standard deviation.

**Figure 9:** Same of figure 8 but for GM experiment.

**Figure 10:** May to August 200 hPa divergence ($s^{-1}$) for GM experiment. Shading denotes those regions where the multimodel ensemble mean is larger in magnitude than the inter-model standard deviation; solid (dashed) lines denote positive (negative) anomalies.

**Figure 11:** May to August sum of the 200 hPa eddy-psi anomalies ($10^6$ $m^2s^{-1}$) of TA and IP experiments.

**Figure 12:** Twenty year running correlation, sliding 1 year the window, from 1901–2000 to 1980–99, between observed Atl3 index and Gulf of Guinea (GG) precipitation index (blue line), Atl3 index and Sahelian precipitation index (black line), Niño3 index and GG precipitation index (red line) and summer Niño3 index and Sahelian precipitation index (green line). All the indexes are calculated for boreal summer season (July to September). Dots denote 95% significant correlations under a Montecarlo test with 500 permutations of the original timeseries.

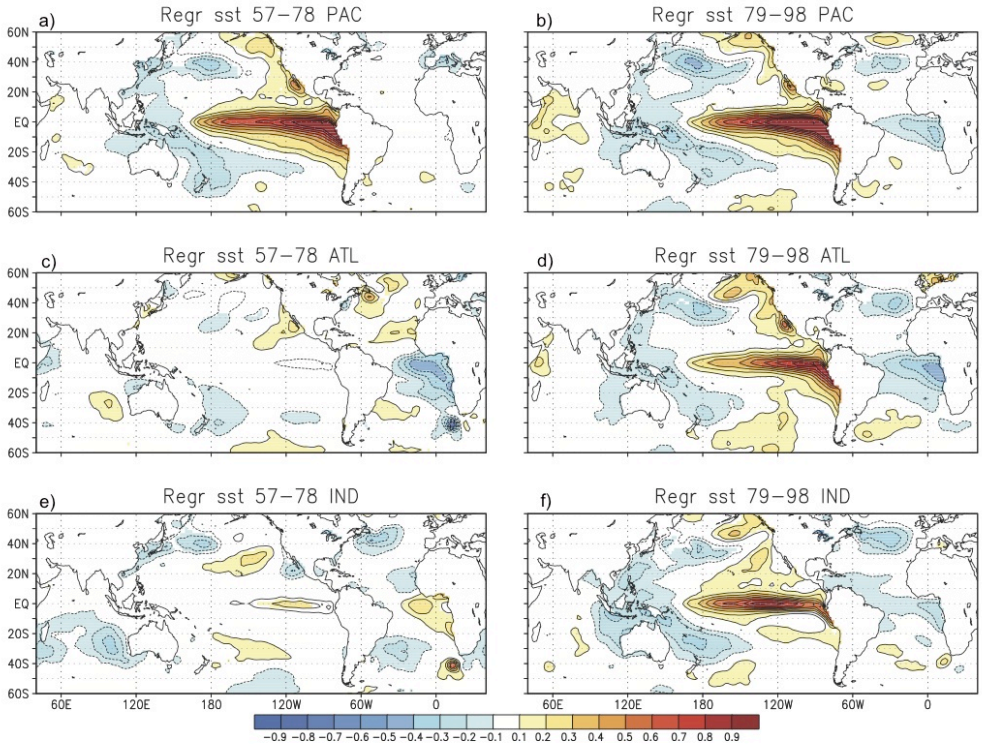
a)
Regr sst 57–78 PAC
b)
Regr sst 79–98 PAC
c)
Regr sst 57–78 ATL
d)
Regr sst 79–98 ATL
e)
Regr sst 57–78 IND
f)
Regr sst 79–98 IND
60N
40N
20N
EQ
20S
40S
60S
60E
120E
180
120W
60W
0
−0.9 −0.8 −0.7 −0.6 −0.5 −0.4 −0.3 −0.2 −0.1 0.1 0.2 0.3 0.4 0.5 0.6 0.7 0.8 0.9

Figure 1